

Experimental Validation of a Real-Time Optimal Controller for Coordination of CAVs in a Multi-Lane Roundabout

Behdad Chalaki, *IEEE Student Member*, Logan E. Beaver, *IEEE Student Member*,
Andreas A. Malikopoulos, *IEEE Senior Member*

Abstract—Roundabouts and other transportation bottlenecks may induce congestion in a traffic system due to driver responses to various disturbances. Research efforts have shown that smoothing traffic flow and eliminating stop-and-go driving can both improve fuel efficiency of the vehicles and the throughput of a roundabout. In this paper, we validate an optimal control algorithm developed earlier in a multi-lane roundabout scenario using University of Delaware’s scaled smart city (UDSSC). We first provide conditions where the solution is optimal. Then, we demonstrate the feasibility of the solution using experiments at UDSSC, and show that the optimal solution completely eliminates stop-and-go driving while preserving safety.

I. INTRODUCTION

With the advent of emerging information and communication technologies, we are witnessing a massive increase in the integration of our energy, transportation, and cyber networks. These advances, coupled with human factors, are giving rise to a new level of complexity in transportation networks [1]. As we move to increasingly complex emerging transportation systems, with changing landscapes enabled by connectivity and automation, future transportation networks could shift dramatically with the large-scale deployment of connected and automated vehicles (CAVs). In 2015, congestion caused people in urban areas in the US to spend 6.9 billion additional hours on the road and to purchase an extra 3.1 billion gallons of fuel, resulting in a total cost estimated at \$160 billion [2]. Traffic accidents have also increased dramatically over the last decades. In 2015, 35,092 people died on US roadways. However, 94% of serious motor vehicle crashes are due to human error [3].

There have been two major approaches that use CAVs to improve both the safety and efficiency of transportation systems. The first approach is based on connectivity and automation being used to reduce vehicle gaps and form high-density vehicle platoons. The idea of introducing these platoons to transportation networks gained momentum in the 1980s and 1990s [4], [5] as a method to alleviate congestion. The second approach is to smooth the flow of traffic to eliminate stop-and-go driving by applying optimal

coordination to traffic bottlenecks. For example, Stern et al. [6] demonstrated how the insertion of a single CAV following a classical control policy into a ring road of human-driven vehicles could diminish stop-and-go waves.

Several efforts have been reported in the literature towards coordinating CAVs to reduce spatial and temporal speed variation of individual vehicles throughout the network. These variations can be introduced to the system through the environment, such as by breaking events, or due to the structure of the road network, e.g., intersections [7], [8], cooperative merging [9]–[11], and speed harmonization [12]. One of the earliest efforts in this direction was proposed by Athans [13] to efficiently and safely coordinate merging behaviors as a step to avoid congestion. Since then, several research efforts have been reported in the literature proposing coordination of CAVs. Most studies have focused on traffic bottlenecks, such as merging roadways, urban intersections, and speed reduction zones. In earlier work, a decentralized optimal control framework was established for online coordination of CAVs in various traffic bottlenecks, e.g., merging roadways, urban intersections, speed reduction zones, and roundabouts. The analytical solution, without considering state and control constraints, was presented in [14] and [15], [16] performed online coordination of CAVs at highway on-ramps, a solution for two adjacent intersections was developed in [17], [18], and roundabouts were explored in [19]. The solution of the unconstrained problem was also validated experimentally at University of Delaware’s scaled smart city (UDSSC) using 10 robotic CAVs for a merging roadway scenario in [20] and for a transportation corridor in [21]. The solution of the optimal control problem which considered state and control constraints was presented in [8] at an urban intersection without considering a rear-end collision avoidance constraint. The conditions under which the rear-end collision avoidance constraint never becomes active are discussed in [12]. A thorough literature review of the methods and challenges of CAV coordination is discussed in [9].

When several roadways must come together, roundabouts generally provide better operational and safety characteristics over other types of intersections [22]–[25]. However, the increase of traffic becomes a concern for roundabouts due to their geometry and priority system - even with moderate demands, some roundabouts may quickly reach capacity [26], [27]. Moreover, all incoming traffic may experience a significant delay if the circulating flow is heavy. Previous research has focused mainly on enhancing roundabout mobility and safety with improved metering, or traffic signal

This research was supported in part by ARPAEs NEXTCAR program under the award number DE-AR0000796 and by the Delaware Energy Institute (DEI). This support is gratefully acknowledged.

The authors are with the Department of Mechanical Engineering, University of Delaware, Newark, DE 19716 USA (emails: {bchalaki; lebeaver; andreas}@udel.edu).

Supplementary information and videos can be found at:
<https://sites.google.com/view/ud-ids-lab/mlrb>

controls [26]–[29]. To investigate the potential of metering signals in improving roundabout operations during rush hour, Hummer et al. [26] tested a metering approach for a signal-lane roundabout model and a two-lane roundabout model with different levels of approaching traffic demand. Martin-Gasulla et al. [28] studied the benefits of metering signals for roundabouts with unbalanced flow patterns. Yang et al. [27] proposed a traffic-signal control algorithm to eliminate the conflict points and weaving sections for multi-lane roundabouts by introducing a second stop line for left-turn traffic. Xu et al. [29] suggested a multi-level control system that combines metering signalization with full actuated control to serve different time periods throughout the day. Zohdi and Rakha [30] showed that by using a cooperative adaptive cruise controller, they could improve the fuel efficiency and reduce the travel delay in a single lane roundabout compared to traditional roundabouts. Bichiou and Rakha [31] proposed an optimization framework for minimizing the travel time and fuel consumption jointly with minimum control effort for CAVs using a numerical solver. They have demonstrated the improvement in fuel efficiency and travel time; however, the method is not real-time implementable due to the computational cost. Finally, [32] and [33] have experimentally validated CAV controllers in a scaled testbed. However, [32] only utilizes 2-3 CAVs for validation of collision avoidance, overtaking, and traffic-jam scenarios. Meanwhile, [33] is applicable to several CAVs in highway driving conditions.

In this paper, we validate an optimal control algorithm developed earlier in a multi-lane roundabout scenario using UDSSC. We first provide the conditions where the solution is globally optimal. Then, we demonstrate the feasibility of the solution using experiments at UDSSC, and show that the optimal solution completely eliminates stop-and-go driving while preserving safety. We implement the solution in real time for 9 CAVs in a multi-lane roundabout with three areas for the potential lateral collision.

The remainder of the paper is organized as follows. In Section II, we introduce our modeling framework. In Section III, we provide the analytical solution of the optimal control problem and the experimental setup in Section IV. Then, we present the results and discussion in Section V, and finally, we draw concluding remarks and discuss future work in Section VI.

II. PROBLEM FORMULATION

A. The Roundabout Scenario

In this work we consider a multi-lane roundabout with three CAV inflows and three areas where lateral collisions between CAVs may occur; this is visualized in Fig. 1. To navigate the roundabout, we define a *control zone*, which starts upstream from the roundabout and ends at each roundabout exit. The control zone has an associated *coordinator*, which stores information about the geometry of the roundabout and the trajectory information of each CAV in the control zone. The coordinator does not make any decisions and only acts as a database.

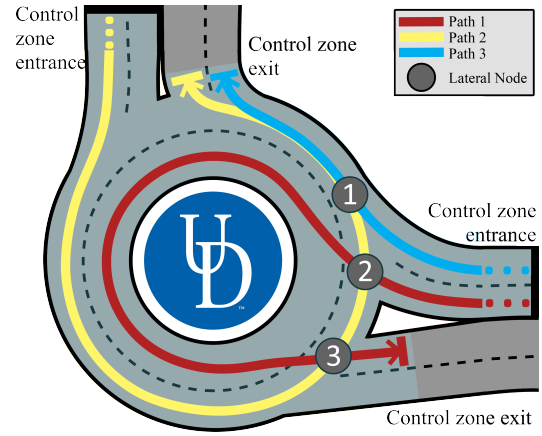


Fig. 1. A schematic of the roundabout scenario. The highlighted control zone continues upstream from the roundabout. There are three conflict points which may result in lateral collisions.

Let $\mathcal{Q}(t) \subset \mathbb{N}$ be the set of CAVs at time $t \in \mathbb{R}^+$ which are inside the control zone. Upon entering the control zone at time $t_i^0 \in \mathbb{R}^+$, CAV $i \in \mathcal{Q}(t)$ retrieves the trajectory information of every other CAV $j \in \mathcal{Q}(t) \setminus \{i\}$ and generates an energy-optimal safe trajectory through the control zone. Then, CAV i broadcasts its trajectory to the coordinator. Finally, when CAV i exits the control zone at time t_i^f , it is removed from the set $\mathcal{Q}(t)$. A detailed discussion of this coordinator framework is presented in [21].

Definition 1. We define each lateral node with a unique index, $n \in \{1, 2, 3\}$, at each area inside the roundabout where there is potential for a lateral collision (Fig. 1).

Definition 2. For each CAV $i \in \mathcal{Q}(t)$, we define \mathcal{N}_i as the set of all lateral nodes on the path of CAV i .

For instance, if CAV i is traveling along path 1 (Fig. 1), the set of collision nodes is $\mathcal{N}_i = \{2, 3\}$.

Definition 3. For each CAV $i \in \mathcal{Q}(t)$, upon entering the control zone at time t_i^0 , we define the set of lateral nodes shared with each CAV $j \in \mathcal{Q}(t_i^0) \setminus \{i\}$ as,

$$\mathcal{C}_{i,j} = \{n \mid n \in \mathcal{N}_i \cap \mathcal{N}_j\}. \quad (1)$$

B. Vehicle Model and Constraints

We represent the dynamics of each CAV $i \in \mathcal{Q}(t)$, with the state equation and initial condition

$$\dot{\mathbf{x}}_i(t) = f(t, \mathbf{x}_i(t), u_i(t)), \quad \mathbf{x}_i(t_i^0) = \mathbf{x}_i^0, \quad (2)$$

where $t \in \mathbb{R}^+$, and $\mathbf{x}_i(t) = [p_i(t), v_i(t)]^T$, $u_i(t)$ are the state and control input of i at time t . Let t_i^0 be the time that i enters the control zone, and $\mathbf{x}_i^0 = [p_i^0, v_i^0]^T$ be the state at this time. We model each CAV i as a double integrator

$$\begin{aligned} \dot{p}_i &= v_i(t), \\ \dot{v}_i &= u_i(t), \end{aligned} \quad (3)$$

where $p_i(t) \in \mathcal{P}_i$, $v_i(t) \in \mathcal{V}_i$, and $u_i(t) \in \mathcal{U}_i$ denote the position, speed and acceleration/deceleration (control input)

of each CAV i inside the control zone. The sets \mathcal{P}_i , \mathcal{V}_i , and \mathcal{U}_i are complete and totally bounded subsets of \mathbb{R} .

For each CAV $i \in \mathcal{Q}(t)$ the control input and speed at time $t \in [t_i^0, t_i^f]$ are bounded by

$$\begin{aligned} u_{i,min} &\leq u_i(t) \leq u_{i,max}, \\ 0 < v_{min} &\leq v_i(t) \leq v_{max}, \end{aligned} \quad (4)$$

where $u_{i,min}$, $u_{i,max}$ are the minimum deceleration and maximum acceleration for each i inside the control zone, and v_{min} , v_{max} are the minimum and maximum speed limits respectively. For simplicity, we do not consider CAV diversity. Thus, in the rest of the paper, we set $u_{i,min} = u_{min}$ and $u_{i,max} = u_{max}$.

Definition 4. For any CAV $i \in \mathcal{Q}(t)$, if there exists a CAV $k \in \mathcal{Q}(t)$ which leads CAV i , we define $d_i(t)$ as the bumper-to-bumper distance from CAV k to CAV i . If no such CAV k leads CAV i , then we let $d_i(t) \rightarrow \infty$.

To guarantee no rear-end collision occurs between CAV $i \in \mathcal{Q}(t)$ and the preceding CAV $k \in \mathcal{Q}(t)$, we impose the following rear-end safety constraint,

$$d_i(t) \geq \delta_i(t), \quad (5)$$

where $\delta_i(t)$ is a predefined safe distance. The minimum safe distance $\delta_i(t)$ is a function of speed,

$$\delta_i(t) = \gamma + \varphi v_i(t), \quad (6)$$

where $\gamma, \varphi \in \mathbb{R}$ are the standstill distance and reaction time, respectively.

Lemma 1. For CAV $i \in \mathcal{Q}(t)$ the inverse function of position, $p_i^{-1}(\cdot)$ exists for all $t \in [t_i^0, t_i^f]$.

Proof. From (4), we have $v_i(t) > 0$ for $t \in [t_i^0, t_i^f]$, which implies that $p_i(t)$ is a strictly increasing function. Thus, $p_i(t)$ is an one-to-one function and its inverse exists. ■

For each CAV $i \in \mathcal{Q}(t)$ the distance to a node $n \in \mathcal{N}_i$ is denoted by the function $l_i : \mathcal{N}_i \rightarrow \mathcal{P}_i$. To guarantee lateral collision avoidance, we impose the following constraint for every CAV $i \in \mathcal{Q}(t)$,

$$\begin{aligned} |p_i^{-1}(l_i(n)) - p_j^{-1}(l_j(n))| &> t_h, \\ \forall n \in \mathcal{C}_{i,j}, \quad \forall j \in \mathcal{Q}(t) \setminus \{i\}, \end{aligned} \quad (7)$$

where $t_h \in \mathbb{R}^+$ is a safe time headway.

Remark 1. The lateral safety constraint, (7) relaxes the first-in-first-out policy between CAVs $i, j \in \mathcal{Q}(t)$, which is common in the literature. We avoid this restriction by incorporating an absolute value into (7).

Next, we formulate a decentralized optimal control problem for each CAV $i \in \mathcal{Q}(t)$ in order to minimize their energy consumption over the interval $t \in [t_i^0, t_i^f]$.

Problem 1. When a CAV $i \in \mathcal{Q}(t)$ enters the control zone, it solves the following optimal control problem:

$$\begin{aligned} \min_{u_i(t) \in \mathcal{U}_i} \quad & \frac{1}{2} \int_{t_i^0}^{t_i^f} u_i^2(t) dt, \\ \text{subject to :} \quad & (3), (4), (5), (7), \\ \text{given} \quad & p_i(t_i^0), v_i(t_i^0), p_i(t_i^f). \end{aligned}$$

To derive the analytical solution of Problem 1, we follow the standard methodology used in optimal control problems with interior point state and control constraints [8], [34], [35]. First, we start with the unconstrained solution to Problem 1. If this solution violates any of the state or control constraints, then it is pieced together with the arc corresponding to the violated constraint. This yields a set of algebraic equations that are solved simultaneously using the boundary conditions of Problem 1 and interior conditions between the arcs. If the resulting solution, which incorporates the optimal switching time between arcs, violates another constraint, then the two arcs are pieced together with a third, which corresponds to the new constraint which has been violated. This yields a larger set of algebraic equations that must be solved simultaneously using the boundary conditions of Problem 1 and the interior point conditions between arcs, including the optimal time and state to switch between them. This process is repeated until a piecewise-continuous state trajectory is found, which is a feasible solution for Problem 1.

In general, there is no analytical expression for the solution of Problem 1 when a safety constrained arc becomes active. Additionally, finding a piecewise-continuous state trajectory that optimally pieces the different arcs together is very computationally challenging, and it may become prohibitively difficult for a CAV to solve the optimal control problem onboard in real time [36].

In our approach, we consider the unconstrained solution to Problem 1, i.e., the solution when the state, control, and safety constraints are neglected. The optimal unconstrained trajectory in this case is [8],

$$p_i(t) = a_i t^3 + b_i t^2 + c_i t + d_i, \quad (8)$$

$$v_i(t) = 3a_i t^2 + 2b_i t + c_i, \quad (9)$$

$$u_i(t) = 6a_i t + 2b_i, \quad (10)$$

with the boundary conditions

$$p_i(t_i^0) = p_i^0, \quad v_i(t_i^0) = v_i^0, \quad (11)$$

$$p_i(t_i^f) = p_i^f, \quad u_i(t_i^f) = 0. \quad (12)$$

To derive an energy-optimal control input that can be computed in real time, we seek to minimize the exit time of CAV $i \in \mathcal{Q}(t)$ from the control zone and impose (8) - (10) as an energy-optimal motion primitive. This results in a new energy-optimal scheduling problem [37].

Problem 2. When a CAV $i \in \mathcal{Q}(t)$ enters the control zone, it derives its minimum travel time such that the resulting trajectory is unconstrained and does not violate any state,

control, or safety constraints.

$$\begin{aligned} \min_{a_i, b_i, c_i, d_i} \quad & t_i^f, \\ \text{subject to:} \quad & (4), (5), (7), \\ & (8), (9), (10), (11), (12). \end{aligned}$$

Thus, each CAV $i \in \mathcal{Q}(t)$ will follow the solution to Problem 2, which generates the minimum travel time and imposes the unconstrained energy-optimal trajectory. That is, the solution of Problem 2 yields the minimum t_i^f such that the generated trajectory is the unconstrained and optimal solution to Problem 1. Note that as (8) is a strictly-increasing cubic polynomial for all $t \in [t_i^0, t_i^f]$, the inverse position (7) has a closed-form representation [37]. Next, we provide the assumptions we imposed in our approach on each CAV $i \in \mathcal{Q}(t)$.

Assumption 1. *There are no errors or delays in the vehicle-to-vehicle and vehicle-to-infrastructure communication.*

Assumption 2. *Vehicle-level control is handled by a low-level controller which can perfectly track the trajectory generated by solving Problem 2.*

The first assumption ensures that we address the deterministic case. It is relatively straightforward to relax this assumption as long as the noise or delays are bounded. The second assumption is to decouple the motion planning and vehicle control, which makes the problem tractable. By tuning the low-level controller, it can be ensured that the prescribed trajectory is followed.

III. ANALYTICAL SOLUTION

We seek to transform Problem 2 into an equivalent formulation which can be solved in real time. First, without loss of generality, we consider the domain of Problem 2 to be $t \in [0, t_i^f]$ and $p_i(t) \in [0, S_i]$, where S_i is the length of the control zone corresponding to CAV i 's path. This results in a new set of boundary conditions,

$$p_i(t_i^0 = 0) = 0, \quad v_i(t_i^0 = 0) = v_i^0, \quad (13)$$

$$p_i(t_i^f) = S_i, \quad u_i(t_i^f) = 0. \quad (14)$$

Next, we substitute (13) into (8) and (9) yielding

$$p_i(t_i^0 = 0) = d_i = 0, \quad (15)$$

$$v_i(t_i^0 = 0) = c_i = v_i^0, \quad (16)$$

which must always hold for Problem 2. Next, we substitute (14) into (10), which yields,

$$u_i(t_i^f) = 6a_i t_i^f + 2b_i = 0. \quad (17)$$

This implies that

$$a_i = -\frac{b_i}{3t_i^f}. \quad (18)$$

Next, we substitute (14) and (18) into (8) yielding

$$p_i(t_i^f) = -\frac{b_i}{3t_i^f} t_i^{f3} + b_i t_i^{f2} + v_i^0 t_i^f = S_i. \quad (19)$$

Hence, equation (19) simplifies to

$$b_i = \frac{3(S_i - v_i^0 t_i^f)}{2t_i^{f2}}. \quad (20)$$

We may further simplify Problem 2 by finding a compact domain of feasible t_i^f by explicitly applying the speed and control constraints. Let $t_{i,\min}^f$ and $t_{i,\max}^f$ denote the lower bound and upper bound on t_i^f respectively, which is imposed by the state and control constraints.

Proposition 1. *For each CAV $i \in \mathcal{Q}(t)$, the lower bound on exit time of the control zone, $t_{i,\min}^f$, is computed as follows*

$$t_{i,\min}^f = \min\{t_{i,u_{\max}}^f, t_{i,v_{\max}}^f\}, \quad (21)$$

where

$$t_{i,u_{\max}}^f = \frac{\sqrt{9v_0^2 + 12S_i u_{\max}} - 3v_0}{2u_{\max}}, \quad (22)$$

$$t_{i,v_{\max}}^f = \frac{3S_i}{v_i^0 + 2v_{i,\max}}. \quad (23)$$

Proof. There are two cases to consider: **Case 1:** CAV i achieves its maximum control input at entry of the control zone, as $u_i(t_i^0) = u_{\max}$. **Case 2:** CAV i achieves its maximum speed at the end of control zone, as $v_i(t)$ is strictly increasing $v_i(t_i^f) = v_{\max}$.

In case 1, by (10), we have

$$u_i(t_i^0 = 0) = 2b_i = u_{\max}. \quad (24)$$

Substituting (20) into (24) and solving for t_i^f , yields the quadratic equation

$$u_{\max} t_i^{f2} + 3v_i^0 t_i^f - 3S_i = 0, \quad (25)$$

which has two real roots with opposite signs, as $t_{i,1}^f t_{i,2}^f = \frac{-3S_i}{u_{\max}} < 0$. Thus, $t_{i,u_{\max}}^f > 0$ is computed by

$$t_{i,u_{\max}}^f = \frac{\sqrt{9v_0^2 + 12S_i u_{\max}} - 3v_0}{2u_{\max}}. \quad (26)$$

For case 2, by (9), we have

$$v_i(t_i^f) = \frac{a_i}{3} t_i^{f2} + \frac{b_i}{2} t_i^f + v_i^0 = v_{\max}. \quad (27)$$

Substituting (18) and (20) into 27 yields

$$v_i(t_i^f) = 3\left(\frac{-b_i}{3t_i^f}\right) t_i^{f2} + 2b_i t_i^f + v_0 = v_{\max}, \quad (28)$$

$$= b_i t_i^f + v_0 = \frac{3(S_i - v_i^0 t_i^f)}{2t_i^f} + v_0 = v_{\max},$$

which simplifies to

$$t_{i,v_{\max}}^f = \frac{3S_i}{v_i^0 + 2v_{\max}}. \quad (29)$$

Thus, our lower bound on t_i^f is given by

$$t_{i,\min}^f = \min\{t_{i,u_{\max}}^f, t_{i,v_{\max}}^f\}. \quad (30)$$

■

Proposition 2. For each CAV $i \in \mathcal{Q}(t)$, the upper bound on exit time of the control zone, $t_{i,\max}^f$, is computed as follows

$$t_{i,\max}^f = \begin{cases} t_{i,v_{\min}} & , \text{ if } 9v_0^2 + 12S_i u_{i,\min} < 0, \\ \max\{t_{i,u_{\min}}^f, t_{i,v_{\min}}^f\} & , \text{ otherwise.} \end{cases} \quad (31)$$

where

$$t_{i,v_{\min}} = \frac{3S_i}{v_0^2 + 2v_{\min}}, t_{i,u_{\min}} = \frac{\sqrt{9v_0^2 + 12S_i u_{\min}} - 3v_0}{2u_{\min}}. \quad (32)$$

Proof. Similar steps can be followed to find the upper bound for $t_{i,\max}^f$.

First, to find $t_{i,u_{\min}}^f$, we have

$$u_{\min} t_i^2 + 3v_0 t_i - 3S_i = 0, \quad (33)$$

which has two positive roots if the discriminant is non-negative, as $t_{i,1}^f t_{i,2}^f = \frac{-3S_i}{u_{\min}} > 0$. Of these we will select the smaller one,

$$t_{i,u_{\min}}^f = \frac{\sqrt{9v_0^2 + 12S_i u_{\min}} - 3v_0}{2u_{\min}}. \quad (34)$$

Note that when $9v_0^2 + 12S_i u_{\min} < 0$ there is no real root of t_i^f which satisfies all of the boundary conditions simultaneously. Thus, the constraint $u(t_i^0) = u_{\min}$ can never become active if (34) is complex, and the lower bound is given by the v_{\min} case. The proof for the v_{\min} case is identical to Proposition 2 and is omitted. ■

Finally, we may write an equivalent formulation of Problem 2, which optimizes a single variable, t_i^f over a compact set $[t_{i,\min}^f, t_{i,\max}^f]$.

Problem 3. When CAV $i \in \mathcal{Q}(t)$ enters the control zone it derives the minimum exit time such that the resulting unconstrained trajectory does not violate any safety constraints.

$$\begin{aligned} & \min_{t_i^f} t_i^f, \\ \text{subject to: } & (5), (7), \\ & (15), (16), (18), (20), \\ & t_i^f \in [t_{i,\min}^f, t_{i,\max}^f]. \end{aligned}$$

Problem 3 can be numerically solved in real time by each CAV $i \in \mathcal{Q}(t)$ upon entering the control zone. In the next section, we describe our experimental testbed and the implementation of the proposed approach.

IV. EXPERIMENTAL SETUP

To experimentally validate our method, experiments were carried out in UDSSC, (Fig. 2) using nine scaled CAVs traveling along three different conflicting paths (Fig. 1). UDSSC is a 1:25 scale testbed designed to replicate real-world traffic scenarios and test cutting-edge control technologies in a safe and scaled environment. UDSSC is a fully integrated smart city, which can be used to validate the efficiency of control and learning algorithms and their applicability in hardware. It utilizes high-end computers, a

VICON motion capture system, and a fleet of scaled CAVs (Fig. 3) to simulate a variety of centralized and decentralized control strategies. Each CAV has a Raspberry Pi 3B with a 1.2 GHz quad-core ARM processor and communicates with the *mainframe* computer (Processor: Intel Core i7 – 6950X CPU @ 3.00 GHz x 20, Memory: 125.8 Gb). UDSSC has been used successfully for coordination of CAVs [20], [21] and implementation of reinforcement learning policies [38], [39].



Fig. 2. The University of Delaware's scaled smart city. The roundabout used in this experiment is in the upper-left side of the image.



Fig. 3. A picture of the connected and automated vehicles in University of Delaware's scaled smart city.

High-level routing is achieved by a multithreaded C++ application which runs on the mainframe computer. The CAV receives its position, speed profile, and the path information from the mainframe and uses a modified Stanley [40] controller to handle lane tracking. Meanwhile, a feed-forward-feedback PID controller [41] tracks the desired speed profile. Medium and low-level control is accomplished on-board each CAV in a purely distributed manner. For further details about UDSSC's hardware see [21].

Each CAV starts their path outside the control zone and applies the Intelligent Driver Model (IDM) [42]. The acceleration command given to a CAV $i \in \mathcal{Q}(t)$ following CAV $k \in \mathcal{Q}(t)$ is

$$u_i = a_{\max} \left(1 - \left(\frac{v_i}{v_{\max}} \right)^\delta - \frac{s_0 + v_i t_h + (v_i(v_i - v_k))^2}{2\sqrt{a_{\max} v_{\max} d_i}} \right)$$

where δ is the acceleration exponent, t_h is the desired time headway, and s_0 is the desired standstill distance.

Upon entering the control zone, CAV $i \in \mathcal{Q}(t)$ determines its trajectory by solving Problem 3 numerically. CAV i , then, follows this fixed trajectory and returns to the IDM controller after exiting the control zone.

Table I gives the parameters used in the experiment such as control zone length, state and control constraints, (4), and safety constraints, (5), (7). The experiments in UDSSC used nine CAVs with three CAV per path (Fig. 1). The experiment was repeated five times to collect multiple data sets and give an estimate on the noise and disturbances present in the system. The CAV inflows were explicitly configured to lead to lateral collisions in the uncontrolled case. Next, we present and discuss the results of these experiments.

TABLE I

PARAMETERS USED FOR THE OPTIMAL CONTROLLER IN UNIVERSITY OF DELAWARE'S SCALED SMART CITY; VALUES ARE GIVEN IN THE 1:25 CITY SCALE.

Parameters	Values	Reference
S_1, S_2, S_3	5.36 m, 5.81 m, 3.78 m	Control zone lengths
v_{\min}, v_{\max}	0.15 m/s, 0.5 m/s	State constraints
u_{\min}, u_{\max}	-0.45 m/s ² , 0.45 m/s ²	Control constraints
γ, ϕ	1 m, 0.27 s	Rear-end safety (5)
t_h	1.0 s	Time headway (7)

V. RESULTS AND DISCUSSION

To validate our proposed controller in UDSSC, several pieces of data were collected throughout the five experiments. First, the position, speed, location within the UDSSC, and a timestamp for each CAV was streamed back to the mainframe at a rate of 20 Hz. Furthermore, the state and time of each CAV entering the control zone were recorded, as well as the computed and achieved exit time. These results are summarized in Table II. Note that the minimum speed of any CAVs across all five experiments is 0.12 m/s (7 mph at full scale), which demonstrates that stop and go driving has been completely eliminated. Additionally, the average CAV speed is 0.42 m/s (24 mph at full scale), which implies that most CAVs are traveling near v_{\max} and must apply minimal control effort.

TABLE II

AVERAGE VELOCITY AND TRAVEL TIME RESULTS FOR THE 5 EXPERIMENTS. RMSE IS NORMALIZED BY TRAVEL TIME FOR EACH CAV.

Experiment	v_{\min} [m/s]	v_{avg} [m/s]	Travel Time RMSE
1	0.16	0.41	2.71 %
2	0.27	0.45	1.54 %
3	0.18	0.41	4.03 %
4	0.12	0.43	1.92 %
5	0.21	0.42	1.38 %

The exit time data for each CAV is visualized in Fig. 4, where the grey bars represent the feasible space of t_i^f , the wide black bars correspond with the solution of Problem 3,

and the thin red bars show the achieved exit time for each CAV. From Table II, the error between desired and actual exit time varies between 2-4%. This error comes from the CAV's ability to track the desired trajectory and shows that Assumption 2 is reasonable for well-tuned CAVs in UDSSC.

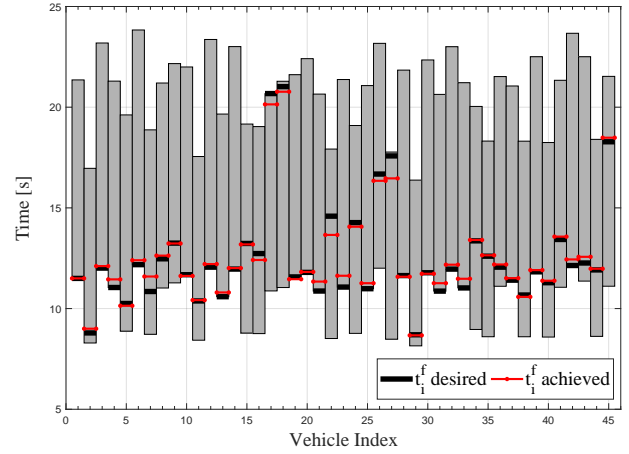


Fig. 4. Estimated and actual arrival time for each vehicle over all experiments. The grey bar shows the range of admissible t_i^f from the state and control constraints. Every 9 vehicles corresponds to a single experiment; they are sorted in ascending order by departure time from the control zone.

The position trajectory of an ego-CAV following path 2 is given in Fig. 5; the ego-CAV's position is denoted by the dashed red line, while the positions of two other CAVs are represented by dotted black lines. The lateral collision constraints are denoted by vertical black bars, and the rear-end safety constraint is the hashed region on the graph. There are two other CAVs shown; one is on Path 3 and merges in front of the ego-CAV at collision node 1 (Fig. 1) and the second CAV leads the ego-CAV on path 2.

Figure 5 demonstrates that for a real CAV Assumption 1 is too strong. The trajectory generated by the ego-vehicle may not violate any constraints, but the actual trajectory violates the rear-end safety constraint by a car length (0.2 m). However, at this speed, the rear-end safety constraint requires a three-car length gap, so a robust control formulation of Problem 3 could likely guarantee collision avoidance. This can also be seen in the lateral collision avoidance constraint in Fig. 5, where a later CAV crosses node 3 in a way that violates the time headway constraint (again, without leading to an actual collision).

Finally, the average, maximum, and minimum speed for each CAV across all experiments are given in Figs. 6 - 8. Each figure corresponds to a single path (see Fig. 1) and is taken over 15 CAV (3 CAVs per path over five experiments). The CAVs' positions are taken directly from VICON and numerically derived using a first-order method.

From Figs. 6 - 8, the average speed for CAVs on each path is very close to constant. Path 1 shows the most variance, which is due to the distance between collision nodes 2 and 3 on path 1 (see Fig. 1). In order for a CAV $i \in \mathcal{Q}(t)$ which is traveling along path 1 to reduce its arrival time

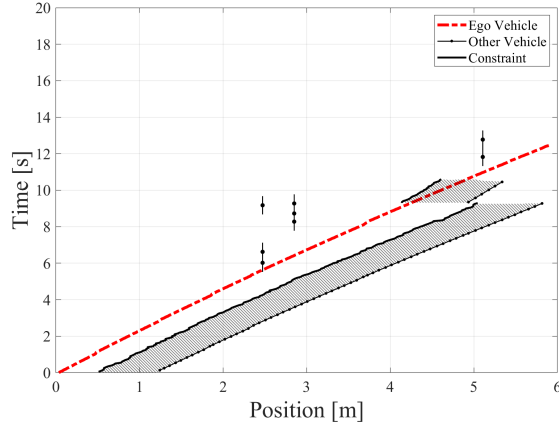


Fig. 5. Position trajectory for the third vehicle entering from path 2 in the 5th experiment. The lateral constraints are shown as vertical lines, and the rear-end safety constraint is the hashed region.

at node 2, it must make a proportionally larger reduction in the value of t_i^f . This is a side effect of enforcing the unconstrained trajectory on each CAV over the entire control zone. Additionally, the entrance to the control zone along path 3 follows a sharp right turn. This results in a relatively lower average trajectories in Fig. 7, as the dynamics of the CAVs reduce their speed while rounding these turns, causing them to enter the control zone at a lower speed.

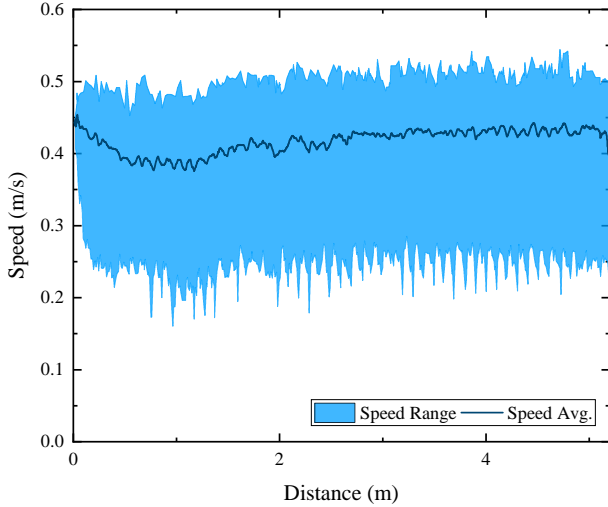


Fig. 6. Maximum, minimum, and average speed of CAVs on the path 1 (Fig. 1) over the control zone length for the five experiments.

VI. CONCLUSION

In this paper, we implemented an optimal control algorithm for coordination of CAVs in a multi-lane roundabout. We demonstrated that our proposed control algorithm can be implemented in real time in a multi-lane roundabout scenario with multiple locations for potential lateral collisions. We experimentally validated the proposed algorithm in UDSSC

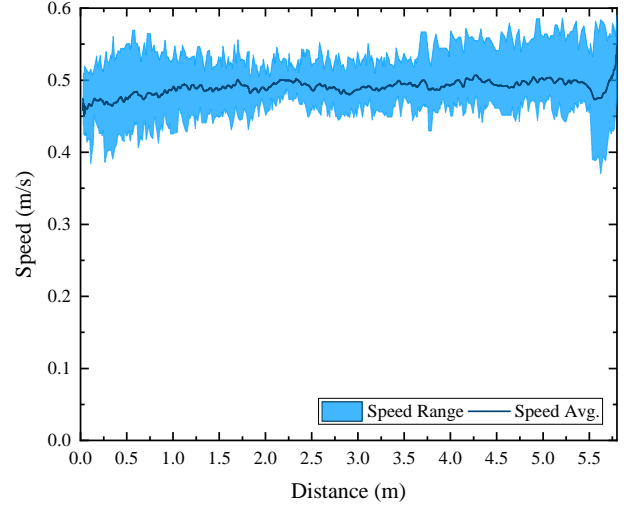


Fig. 7. Maximum, minimum, and average speed of CAVs on the path 2 (Fig. 1) over the control zone length for the five experiments.

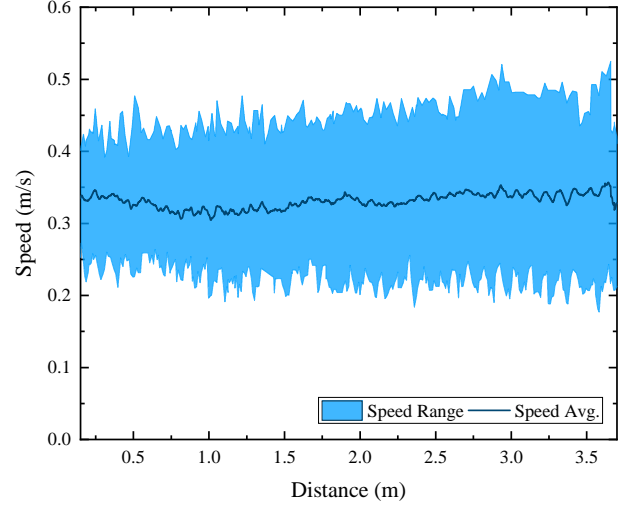


Fig. 8. Maximum, minimum, and average speed of CAVs on the path 3 (Fig. 1) over the control zone length for the five experiments.

using 9 CAVs over a series of 5 experiments. We demonstrated that the proposed algorithm eliminates stop-and-go driving while avoiding collisions between CAVs.

The next step is to enhance the problem formulation to account for noise, disturbances, and communication delays in the CAVs. Exploring the tradeoff between the state and control constraints (increasing the feasible space of t_i^f) and the safe lateral time headway (decreasing the feasible space of t_i^f) is another interesting direction for future research.

REFERENCES

- [1] A. A. Malikopoulos, "A duality framework for stochastic optimal control of complex systems," *IEEE Transactions on Automatic Control*, vol. 61, no. 10, pp. 2756–2765, 2016.
- [2] B. Schrank, B. Eisele, T. Lomax, and J. Bak, "2015 Urban Mobility Scorecard," Texas A& M Transportation Institute, Tech. Rep., 2015.

- [3] S. Singh, "Critical reasons for crashes investigated in the national motor vehicle crash causation survey," Tech. Rep., 2015.
- [4] S. E. Shladover, C. A. Desoer, J. K. Hedrick, M. Tomizuka, J. Walrand, W.-B. Zhang, D. H. McMahon, H. Peng, S. Sheikholeslam, and N. McKeown, "Automated vehicle control developments in the PATH program," *IEEE Transactions on Vehicular Technology*, vol. 40, no. 1, pp. 114–130, 1991.
- [5] R. Rajamani, H.-S. Tan, B. K. Law, and W.-B. Zhang, "Demonstration of integrated longitudinal and lateral control for the operation of automated vehicles in platoons," *IEEE Transactions on Control Systems Technology*, vol. 8, no. 4, pp. 695–708, 2000.
- [6] R. E. Stern, S. Cui, M. L. D. Monache, R. Bhadani, M. Bunting, M. Churchill, N. Hamilton, H. Pohlmann, F. Wu, B. Piccoli, et al., "Dissipation of stop-and-go waves via control of autonomous vehicles: Field experiments," *arXiv preprint arXiv:1705.01693*, 2017.
- [7] J. Lee and B. Park, "Development and Evaluation of a Cooperative Vehicle Intersection Control Algorithm Under the Connected Vehicles Environment," *IEEE Transactions on Intelligent Transportation Systems*, vol. 13, no. 1, pp. 81–90, 2012.
- [8] A. A. Malikopoulos, C. G. Cassandras, and Y. Zhang, "A decentralized energy-optimal control framework for connected automated vehicles at signal-free intersections," *Automatica*, vol. 93, pp. 244–256, 2018.
- [9] J. Rios-Torres and A. A. Malikopoulos, "Automated and Cooperative Vehicle Merging at Highway On-Ramps," *IEEE Transactions on Intelligent Transportation Systems*, vol. 18, no. 4, pp. 780–789, 2017.
- [10] I. A. Ntousakis, I. K. Nikolos, and M. Papageorgiou, "Optimal vehicle trajectory planning in the context of cooperative merging on highways," *Transportation Research Part C: Emerging Technologies*, vol. 71, pp. 464–488, 2016.
- [11] L. Zhao and A. A. Malikopoulos, "Decentralized optimal control of connected and automated vehicles in a corridor," in *2018 21st International Conference on Intelligent Transportation Systems (ITSC)*. IEEE, 2018, pp. 1252–1257.
- [12] A. A. Malikopoulos, S. Hong, B. Park, J. Lee, and S. Ryu, "Optimal control for speed harmonization of automated vehicles," *IEEE Transactions on Intelligent Transportation Systems*, vol. 20, no. 7, pp. 2405–2417, 2019.
- [13] M. Athans, "A unified approach to the vehicle-merging problem," *Transportation Research*, vol. 3, no. 1, pp. 123–133, 1969.
- [14] J. Rios-Torres, A. A. Malikopoulos, and P. Pisu, "Online Optimal Control of Connected Vehicles for Efficient Traffic Flow at Merging Roads," in *2015 IEEE 18th International Conference on Intelligent Transportation Systems*, 2015, pp. 2432–2437.
- [15] J. Rios-Torres and A. A. Malikopoulos, "Automated and Cooperative Vehicle Merging at Highway On-Ramps," *IEEE Transactions on Intelligent Transportation Systems*, vol. 18, no. 4, pp. 780–789, 2017.
- [16] I. A. Ntousakis, I. K. Nikolos, and M. Papageorgiou, "Optimal vehicle trajectory planning in the context of cooperative merging on highways," *Transportation Research Part C: Emerging Technologies*, vol. 71, pp. 464–488, 2016.
- [17] A. Mahbub, L. Zhao, D. Assanis, and A. A. Malikopoulos, "Energy-optimal coordination of connected and automated vehicles at multiple intersections," in *Proceedings of 2019 American Control Conference*, 2019, pp. 2664–2669, 2019.
- [18] B. Chalaki and A. A. Malikopoulos, "An optimal coordination framework for connected and automated vehicles in two interconnected intersections," in *Proceedings of 2019 IEEE Conference on Control Technology and Applications*, 2019, 2019, pp. 888–893.
- [19] L. Zhao, A. A. Malikopoulos, and J. Rios-Torres, "Optimal control of connected and automated vehicles at roundabouts: An investigation in a mixed-traffic environment," in *15th IFAC Symposium on Control in Transportation Systems*, 2018, pp. 73–78.
- [20] A. Stager, L. Bhan, A. A. Malikopoulos, and L. Zhao, "A scaled smart city for experimental validation of connected and automated vehicles," in *15th IFAC Symposium on Control in Transportation Systems*, 2018, pp. 130–135.
- [21] L. E. Beaver, B. Chalaki, A. Mahbub, L. Zhao, R. Zayas, and A. A. Malikopoulos, "Demonstration of a time-efficient mobility system using a scaled smart city," *Vehicle System and Dynamics*, *arXiv preprint arXiv:1903.01632*, 2020 (in press).
- [22] A. Flannery and T. Datta, "Operational performance measures of american roundabouts," *Transportation Research Record*, vol. 1572, no. 1, pp. 68–75, 1997.
- [23] A. Flannery, L. Eleftheriadou, P. Koza, and J. McFadden, "Safety, delay, and capacity of single-lane roundabouts in the united states," *Transportation Research Record*, vol. 1646, no. 1, pp. 63–70, 1998.
- [24] H. M. Al-Madani, "Dynamic vehicular delay comparison between a police-controlled roundabout and a traffic signal," *Transportation Research Part A: Policy and Practice*, vol. 37, no. 8, pp. 681–688, 2003.
- [25] V. P. Sisiopiku and H.-U. Oh, "Evaluation of roundabout performance using sidra," *Journal of Transportation Engineering*, vol. 127, no. 2, pp. 143–150, 2001.
- [26] J. E. Hummer, J. S. Milazzo, B. Schroeder, and K. Salamati, "Potential for metering to help roundabouts manage peak period demands in the united states," *Transportation research record*, vol. 2402, no. 1, pp. 56–66, 2014.
- [27] X. Yang, X. Li, and K. Xue, "A new traffic-signal control for modern roundabouts: method and application," *IEEE Transactions on Intelligent Transportation Systems*, vol. 5, no. 4, pp. 282–287, 2004.
- [28] M. Martin-Gasulla, A. García, and A. T. Moreno, "Benefits of metering signals at roundabouts with unbalanced flow: patterns in spain," *Transportation Research Record*, vol. 2585, no. 1, pp. 20–28, 2016.
- [29] H. Xu, K. Zhang, and D. Zhang, "Multi-level traffic control at large four-leg roundabouts," *Journal of Advanced Transportation*, vol. 50, no. 6, pp. 988–1007, 2016.
- [30] I. H. Zohdy and H. A. Rakha, "Enhancing roundabout operations via vehicle connectivity," *Transportation Research Record*, vol. 2381, no. 1, pp. 91–100, 2013.
- [31] Y. Bichiou and H. A. Rakha, "Developing an optimal intersection control system for automated connected vehicles," *IEEE Transactions on Intelligent Transportation Systems*, vol. 20, no. 5, pp. 1908–1916, 2018.
- [32] K. Berntorp, T. Hoang, and S. Di Cairano, "Motion planning of autonomous road vehicles by particle filtering," *IEEE Transactions on Intelligent Vehicles*, vol. 4, no. 2, pp. 197–210, 2019.
- [33] N. Hyaldmar, Y. He, and A. Porok, "A fleet of miniature cars for experiments in cooperative driving," in *Proceedings of the IEEE International Conference on Robotics and Automation*, 2019.
- [34] A. E. Bryson and Y. C. Ho, *Applied optimal control: optimization, estimation and control*. CRC Press, 1975.
- [35] I. M. Ross, *A primer on Pontryagin's principle in optimal control*. Collegiate publishers, 2015.
- [36] W. Xiao, C. G. Cassandras, and C. Belta, "Decentralized merging control in traffic networks with noisy vehicle dynamics: a joint optimal control and barrier function approach," in *2019 IEEE Intelligent Transportation Systems Conference (ITSC)*. IEEE, 2019, pp. 3162–3167.
- [37] A. A. Malikopoulos and L. Zhao, "Optimal path planning for connected and automated vehicles at urban intersections," in *Proceedings of the 58th IEEE Conference on Decision and Control*, Published, (see IDS site for publication information).
- [38] K. Jang, E. Vinitzky, B. Chalaki, B. Remer, L. Beaver, A. A. Malikopoulos, and A. Bayen, "Simulation to scaled city: zero-shot policy transfer for traffic control via autonomous vehicles," in *Proceedings of the 10th ACM/IEEE International Conference on Cyber-Physical Systems*, 2019, pp. 291–300.
- [39] B. Chalaki, L. Beaver, B. Remer, K. Jang, E. Vinitzky, A. Bayen, and A. A. Malikopoulos, "Zero-shot autonomous vehicle policy transfer: From simulation to real-world via adversarial learning," *arXiv preprint arXiv:1903.05252*, 2019.
- [40] S. Thrun, M. Montemerlo, H. Dahlkamp, D. Stavens, A. Aron, J. Diebel, P. Fong, J. Gale, M. Halpenny, G. Hoffmann, K. Lau, C. Oakley, M. Palatucci, V. Pratt, P. Stang, S. Strohband, C. Dupont, L. E. Jendrossek, C. Koelen, C. Markey, C. Rummel, J. van Niek-erk, E. Jensen, P. Alessandrini, G. Bradski, B. Davies, S. Ettinger, A. Kaehler, A. Nefian, and P. Mahoney, "Stanley: The robot that won the DARPA Grand Challenge," *Springer Tracts in Advanced Robotics*, 2007.
- [41] M. W. Spong, S. Hutchinson, and M. Vidyasagar, "Robot Dynamics and Control Second Edition," Tech. Rep., 2004.
- [42] M. Treiber, A. Hennecke, and D. Helbing, "Congested traffic states in empirical observations and microscopic simulations," *Physical review E*, vol. 62, no. 2, p. 1805, 2000.